# Understanding the formation of AgBi nanoalloys from a structural and energetic perspective: a theoretical study

Rafael Añez[1], L. Cabral[2], E. Z. da Silva[2], Elson Longo[3], Juan Andrés[4], Miguel A. San-Miguel[5]

[1]Laboratorio de Química Física y Catálisis Computacional, Centro de Química, Instituto Venezolano de Investigaciones Científicas, Caracas 21827, Venezuela

[2]Institute of Physics "Gleb Wataghin" (IFGW), State University of Campinas, 13083-859 Campinas, SP, Brazil

[3]CDMF-UFSCar, Universidade Federal de São Carlos, P.O. Box 676, 13565-905, São Carlos, São Paulo, Brazil.

[4]Departamento de Química Física i Analítica, Universitat Jaume I, 12071, Castelló de la Plana, Spain.

[5]Institute of Chemistry, State University of Campinas-Unicamp, 13083-970 Campinas, SP, Brazil

ABSTRACT

Alloying metals which are not miscible at the bulk solid phase is an efficient way to diversify the function of materials attracted great interest due to their distinctive electronic, optical, catalytic, and magnetic properties compared to pure metal. But in depth understanding of the diffusion process inside the alloying materials is rather limited, especially at the atomic level. A typical example is the Ag-Bi nanoalloy. Then, periodic DFT calculations, at the GGA level, have been performed to understand the formation of Ag-Bi nanoalloys. The calculated values of segregation energy indicate that the interface between Ag and Bi plays a crucial role in the stabilization of the Ag doped with Bi atom. The strong interaction at the interface between the Bi and Ag atoms tends to produce structural changes in both surfaces, situation more accentuated in the Bi surface due to its less compact structure. The interface helps to the migration of the Bi atoms from the Ag surface to the Ag bulk, a segregation process which is very difficult to occur on a clean surface due to the high density of the Ag cubic phase. However, on clean surfaces of Bi the insertion of Ag atoms is more thermodynamically favorable with concomitant changes on the cell parameters to be capable to form a chemical bond between Ag and Bi.

Corresponding authors: *E-mail address: rafael.anez@gmail.com

Fax: +58 212 5041350

Phone number: +58 212 5041741

Keywords:

## INTRODUCTION

Nanoalloys represent an interesting field of research and their development of low dimensional materials has become very active and multidisciplinary because of the remarkable properties of these nanostructured systems [1-4]. Bimetallic nanoparticles (BNs), formed by the mix of two metals to form nanoalloys, have been widely studied in the last decade due to their unique applications in various fields as catalysis [5-7] and medicine [8-15]. Not surprisingly, the properties of such BN structures depend strongly not only on the elemental composition and particle morphology but also on how the two metals are organized in the alloy structure, which are crucial to precisely tuning its properties and functions. By controlling the way how the metals mix together at the nanoscale, the metals exhibit better performances when they form a nanoalloy [16], which can be associated to different effects such as: quantum size, surface and the synergism between the two metals [2,17-21]. Researchers have gained more attention in developing new techniques to produce BNs with different metals and compositions which has opened a new field in the area of the nanoparticle synthesis. One interesting situation observed in the BNs synthesis is the fact that at nanoscale, their formation process does not follow the rules occurring at macroscopic scale. The miscibility restriction that in general controls the formation of alloys at macroscopic level, is not accomplished along the formation of alloys at the nanoscale level. Two examples of the latter are Cu-Pd and Ni-Pd which are immiscible in the bulk phase but readily mix in finite clusters [22, 23].

Bi and Ag metals are two very attractive metals for different applications such as catalytic environmental remediation [24, 25], electrochemical sensing [26, 27], medicine [28, 29] and so on. However, the formation of Bi-Ag BNs has been scarcely studied due principally to the low solubility that these metals display [30], situation that could be attributed to their different crystalline structures (rhombohedral and cubic phases for Bi and Ag, respectively). Recent studies have shown that BNs of Bi-Ag can be synthesized or obtained by different experimental techniques. Ruiz-Ruiz et al. [31] prepared Bi-Ag BNs by a mechanochemical reduction method under room temperature conditions. Using different experimental techniques, the authors obtained predominant ordered-mixing structures of $Ag_x$-$Bi_{1-x}$ nanoalloys in a wide range of Ag molar fraction (x = 0.1 to 0.5). The authors point out that the structural similitude between the rhombohedral lattice of Bi ($\alpha = 57.23°$, a = 4.75 Å) and that of the metastable hexagonal phase of Ag ($\alpha = 60°$, a = 4.08 Å) could help to the mixing both metals. These results seem to indicate that at nanoscale dimensions there is not a limiting factor to produce Bi-Ag BNs at room temperature. On the other hand, new techniques as the irradiation of metal oxides by an electron or femtosecond laser beam have been used to generated Ag and Bi nanoparticles [32-34]. Under a femtosecond laser beam and using the $Ag_2WO_4$ and $NaBiO_3$ as precursors, Machado et al. [35] obtained Bi-Ag BNs. The controlled nucleation and growth of the Ag-Bi BNs occur in *situ* during the irradiation process. These Ag-Bi nanoalloys can assume a randomly mixed structure with up to 6 ± 1 atom % of Bi solubilized into a face-centered cubic structure of Ag with superior bactericidal properties.

A major challenge is to develop a mechanistic understanding of the growth and formation of these complex nanostructures, because physical and chemical properties of such nanostructures strongly not only on the elemental composition, surface structure, and morphology, but also on how the two elements are organized in the nanoalloy structure. Scientifically, a general physics-based model is required for understanding the nature and formation of nanoalloys. First-principles calculations can provide effective and robust descriptors to represent the features of materials in the complex compositional, structural and electronic spaces. In this context, Farsi and Deskins [36] studied the segregation energies for alloys involving Pt, Pd, Ir, and Rh as host and transition metals as dopants by means of periodic density functional theory (DFT) calculations. The authors found that segregation energies are very dependent on the exposed surface at the morphology. Also, the authors compared bulk and sub-surface segregation energies (segregation from the bulk or from the sub layer) and found the segregation trends to be very similar between the two segregation processes. Liberto et al. [37] studied the nitrogen doping in co-exposed (001)-(101) anatase $TiO_2$ surfaces using a hybrid functional in the context of periodic DFT calculations. Their results indicated that in the interface, the formation of N-impurities is energetically favored for both substitutional and interstitial doping. These studies show how quantum calculations are able to determine, from a thermodynamic point of view, the effect produced by the substitution of atoms in particular crystalline network, both in the surface and bulk, and how the interface can modify the stability of these substitutions, situations which must play an important role in the first stages of the BNs formation.

The correlations between size, morphology, and composition of BNs and their physicochemical properties have been well demonstrated, however, the doping processes and their positions inside the nanoalloy are not well understood. Moreover, the phase segregation and distribution of metal atoms are presently lacking. These unresolved issues are mainly due to technical limitations in characterizing the alloy atom distribution at the atomic level [38-41]. Thermodynamics may drive what type of structure forms in a BN, and modeling can be used to predict such structures. Taking into account the above considerations and the scarce experimental investigations in relation with the nature of the Ag-Bi BNs, in this work we study the formation of Ag-Bi nanoalloys from a theoretical point of view using periodic DFT calculations.

The main aim is to investigate the structure, energetic, and electronic changes produced by the substitution of Ag by Bi and segregation processes at both bulk and surfaces.

## COMPUTATIONAL DETAILS AND MODEL SYSTEMS

All the calculations were carried out using Vienna *ab initio* simulation package (VASP) [42, 43] version 5.4.4. The Kohn–Sham equations were solved within the generalized gradient approximation (GGA), as proposed by Perdew-Burke-Ernzerhof (PBE) [44]. The projector-augmented wave (PAW) method of Blöchl [45] in the formulation of Kresse and Joubert [46] was applied to describe electron-ion interactions. The PAWs for Bi and Ag have $6s^2 6p^3$ and $4d^{10} 5s^1$ valence electrons, respectively. The bulks of the Bi (hexagonal) and Ag (cubic) phases were optimized starting from the experimental values [47, 48] with a cutoff of 500 eV. The optimized parameters (see Table 1) are in good agreement with the experimental values displaying percent errors around 2 % which are

typical for the GGA functionals [49, 50]. The convergence with k-point sampling was tested and a Monkhorst–Pack mesh (including the gamma point) of 6x6x6 and 6x6x2 k-points were enough to give a converged total energy (5 meV/atom) of the Ag and Bi bulks, respectively.

Insert table 1

We have performed a systematic study of the (100) surfaces of Ag and Bi metals. The bulks were cut on the (100) direction generating two slabs (see figure 1), a 2x3 cell with 5 atomic planes for the Ag (60 atoms) and a 2x1 cell with 9 atomic planes (36 atoms), respectively. The (100) direction was chosen for both surfaces since it has a low Miller index and the surface vectors of both surfaces match correctly which allows to create the interface. The difference between the number of atoms between both cells is due to the smaller atomic density of the Bi bulk, per layer on the (100) surface the Ag has three times the number of atoms that has the Bi surface. The surface vectors were v = 8.293 and 9.160 Å and u = 12.440 and 12.135 Å for the Ag and Bi surfaces, respectively. The k-point sampling was optimized for the slabs and a 3x2x1 distribution displayed be enough to reach a convergence of the total energy per atom (5 meV/atom) for both surfaces.
It is important to note that segregation energy also depends on the alloy's composition and depending on how many atoms are being segregated. In the present study we modeled a single impurity (dopant) in the host metal. Segregation energy ($E_{seg}$), which is defined as the total energy difference between the states with one atom doping the surface atomic layers and, in the bulk, is calculated by the direct difference between the total anergy of the doped systems as follow

$$E_{seg} = E_{(SupX+AtomY,1st\ or\ 2nd\ layer)} - E_{(SupX+AtomY,3rd\ layer)} \quad (1)$$

Where $E_{(SupX+AtomY,3rd\ layer)}$ is the total energy of the surface doped in the third layer and $E_{(SupX+AtomY,1st\ or\ 2nd\ layer)}$ is the total energy of the surface doped in the first or second layer. Previous works showed how the surface with a doped atom in the third layer correctly simulates the bulk environment and has a negligible effect on the segregation energy results [51, 52]. This model may explain these surface segregation processes, and can be used to make predictions of alloy segregation.

From a thermodynamic point of view, a positive value of $E_{seg}$ indicates that the doping atom has a tendency to remain inside the bulk, while a negative value suggests that the doping atom segregates towards the surface. With the aim to explore the influence of the interface between Ag and Bi on the values of $E_{seg}$, the same analysis is carrying out in an interface formed for both surfaces. For that, an interface is formed with average vectors of the Bi and Ag surfaces which leads to a cell with surface vectors of 8.73 and 12.29 Å and 14 atomic planes, 5 Ni planes and 9 Bi planes. A *vacuum* of 15 Å thickness is imposed for surfaces and interfaces with the aim to avoid the interaction between consecutives cells due to the periodicity. Although to Γ point was enough to reach convergence in the total energy for the interface, a 3x2x1 sample mesh including the Γ point was used to avoid inconsistencies with the results obtained for the Bi and Ag surfaces. All structure optimizations were tested in the context of spin polarized calculation in order to explore the most stable electronic configuration of the systems. The obtained results showed that paramagnetic states are the more stable electronic configurations for all the systems studied in this work. For that situation where the reconstruction affected the structure of

the surface or the interface (especially in the Bi surface which suffered the larger reconstruction), different positions for the doping atom were tested and the more stable situation were chosen in all the cases.

Insert figure 1

## RESULTS AND DISCUSSION

### Surfaces and interfaces

The optimization of the Ag (100) surface does not produce significant changes in its structure. A slight increase in the interlayer distances is the effect produced for the optimization in the five layers slab of the Ag (100) surface. This is not the case of the Bi (100) surface, the surface structure suffers a strong distortion due to the optimization (see figure 2). The hexagonal bulk of Bi is formed by bilayers of atoms parallel to the (001) surface in which each atom is bonded to six Bi atoms, covalently bonded to three Bi atoms of the same bilayer at a distance of 3.10 Å and weakly bonded with three Bi atoms of the adjacent bilayer at a distance of 3.59 Å (the distances were obtained from our optimized bulk). Since in the Bi (100) surface the bilayers are perpendicular to the surface, Bi atoms tend to improve the interaction with those atoms bonded at 3.59 Å, therefore, the strong reconstruction is not an unexpected result and it has been previously discussed in the literature [53, 50]. Although a cell with nine layers seem to be enough thickness, a cell with 16 layers was optimized and the surface structure compared with the nine layers cell. The structural parameters for both surfaces do not display significant differences, then a nine layers cell seem to be enough to mimic the Bi (100) surface.

Insert figure 2

Previous to the optimization process, the surfaces were placed such that the distance between the nearest Bi and Ag atoms was not smaller than 2.6 Å, distance close to the experimental bond distances of the Bi and Ag diatomic molecules (2.53 and 2.66 Å for the $Ag_2$ and $Bi_2$, respectively) [55]. Figure 3 displays the optimized structure for the interface formed with the nine layers cell of the Bi (100) surface and the five layers cell of the Ag (100) surface. The interface formation energy, calculated from the values of the total energy of the surfaces and the interface, is -988 mJ $m^{-2}$ (QUE UNIDADES SON ESTAS?), which indicates a high stability of this interface model with respect to the separated surfaces. The stability of the interface can be attributed to the relative strength of the involved bonds, the energy of the Bi-Ag bond (193 kJ $mol^{-1}$) is similar to the Bi-Bi (200 kJ $mol^{-1}$) and stronger than the Ag-Ag (160 kJ $mol^{-1}$) [56], making more stable the interface with respect to the separated clean surfaces. However, the compact structure of the Ag bulk plays an important role in the interface formation. While the Ag (100) surface suffers only a weak distortion, the Bi surface near to the contact region is strongly distorted. The two first layers of the Bi surface go to the Ag surface and form an atomic Bi layer on the Ag (100) surface. The distances among these Bi atoms and the surface Ag atoms are larger than the distances of the Ag atoms at the (100) surface which, in addition with the strong Bi-Ag interaction, produces an elongation in the Ag-Ag distances on the

(100) surface, the distance between Ag atoms bonded to the Bi atom (but non bonded between them) increase from 4.10 to 4.30 Å, which is even larger than those observed in the optimized Ag bulk. In order to explore how the interaction distances change in the Bi slab at the interface, an analysis of the number of interaction distances less than 3.7 Å was carried out for the bulk (a bulk cell with 36 atoms was used), the surface and the Bi slab of the interface after the optimization process. The corresponding results are presented in Figure 4, and analysis renders that the number of interaction distances increases as the distortion of the cell increases. This is indicative of the transformation from a well ordered arrangement at the bulk to a distorted structure (amorphization) at the interface for the Bi substrate, i.e. an order-disorder transition. Machado et al. [35] found that nanoparticles of Ag with a 6 % atomic Bi concentration in a cubic phase, produced by the femtosecond laser irradiation, displaying an elongation of the (111) interplanar distance of 4.2 % approximately. This increases can be associated to an expansion of the face centered cubic crystalline lattice of metallic Ag to accommodate Bi atoms; but in our case we can sense display how the interface plays a crucial role in the first stage of the segregation process and the formation of Ag-Bi moiety provokes the increases of the distances Ag-Ag at the (100) surface.

The structure of the Bi (100) surface not only changes with the interface formation but also the electronic properties are modified. Figure 5 displays the density of state (DOS) of the Ag and Bi bulk, (100) clean surfaces and, the Bi and Ag (100) surfaces at the interface. An analysis of the results points out that the Ag (100) surface maintains the electronic structure of its bulk phase, but the Bi (100) surface lost great part of its electronic characteristics, situation even evident in the clean surface due to the strong reconstruction suffered. Then, despite the stronger bond energy of the Bi-Bi and Bi-Ag interactions, the compact packing of the Ag cubic phase and the lower atomic density of the Bi hexagonal phase lead to a complete reconstruction of the Bi (100) surface while the Ag (100) surface is maintained with few changes. Indifferently of the energetic processes involved in the BNs formation, from a structural point of view the interface seems to favor the cubic phase of the Ag substrate.

## Segregation energy

### Segregation energy of Ag in Bi

Figure 6 displays the segregation energy of Ag in a clean surface of Bi and in the Bi surface at the interface. In both cases, the Ag prefers to stay near to the surface which is in concordance to the fact that Ag does not display detectable solubility in Bi [57]. At the clean surface, the substitution of a Bi atom in the first layer is the less stable than the substitution in the second or third layer. Figure 7 shows the optimized structures for the substitution of a Bi by a Ag atom in the first, second or third layer of a clean Bi (100) surface. The stability of the surface after the substitution depends of the capacity of the Ag atom to form effective interactions with the Bi atoms. In the first layer, the Ag atom penetrates to the sub layers searching for a better interaction with the Bi atoms. This movement provokes a strong distortion in the surface increasing the slab energy. The dependence of the slab stability with respect to the effective interaction of the Ag atom with the surface, can be observed even for the substitution in more internal layers. Despite

in the second layer the Ag atom interacts with a smaller number of Bi atoms than in the third layer, the interaction distances are shorter (~ 3.01 versus 3.10 Å for the second and third layer, respectively) improvement the Ag-Bi interaction and herein stabilizing the surface. These observations indirectly indicate the formation of a chemical bond between Ag and Bi.

These results suggest that in the case of the nanoalloy formation where Ag atoms substitute the Bi atoms in the hexagonal phase, structural parameters must change in order to improve the interaction between the Bi and Ag atoms which, in turn, would generate a strong stabilization of the nanoparticle.

A detailed analysis of diffraction peaks carried out by Ruiz-Ruiz et al. in Ref. 31 of $Ag_x$-$Bi_{1-x}$ nanoalloys showed that the lattice of the Bi matrix gets strained (contracted), when substitutional insertion of Ag molar fractions smaller than 0.2 to 0.3 occur in the Bi matrix. Then, Ag atoms can contract the lattice of the Bi matrix generating a favorable environment to improve the interaction with the Bi atoms which would favor the movement of the Ag atoms to the Bi bulk.

From a qualitative point of view, the interface only changes the stability of the surface substituted in the first layer (see red line figure 6) which in this case becomes more stable than the surface substituted in the third layer. The same distortion produced in the clean surface occurs in the Bi surface at the interface but the situation is stabilized because Bi atoms move to the surface and interact with the Ag surface (see figure 8 b). This system gains energy due to the interaction among the Bi atoms and the Ag surface, interactions highly favored energetically as was observed in the interface formation. Then, the interface favors the segregation energy inducing Ag atoms go to the surface.

SEGREGATION ENERGY OF Bi IN Ag

Figure 9 displays the segregation energy of Bi in a clean surface of Ag and in the Ag surface at the interface. As indicates the black line in figure, in a clean surface the Bi atom prefers to stay at the surface. In comparison with the Bi surfaces when were doped with a Ag atom, the Ag surfaces do not suffer a strong distortion (see figure 10) which can be attribute to the more compact network of the Ag cubic phase. However, it is evident the local distortion produced by the Bi atom. Interatomic distances between the Ag atoms, parallel to the surface and bonded to the Bi atom, increased which indicate the stress produce by the doping. In the first layer, Bi atom can accommodate in a better way stabilizing the interaction between the Bi and Ag atoms of the layer. The repulsive effects due to the large atomic radius of the Bi atom make the first layer, the most stable place to the Ag substitution in comparison with the doping in the sub surface layers. The relative stability of the segregation energy is, as occurred in the Bi surfaces, altered by the interface formation. However, the interface does not stabilize the first layer substitution, contrary, the interface disfavors the segregation energy. Substitution of one Ag atom by one Bi atom in the first layer, breaks the strong stability generated when the interface is

formed increasing the total energy of the interface and so the segregation energy is disfavored. As it is showed in figure 11 b, interaction distances between the Bi atoms of the Bi surface layer interact strongly with the Bi atoms bonded to the Ag surface indicating a decreasing in the interface stability near to the doping zone.

For the interface doped in the second Ag layer, an interesting situation is found. Even at 0 K temperature in which the calculations are carried out, the distortion produced by this substitution induces a strong reconstruction of the interface. This distortion makes possible the migration of Bi atoms to the first Ag layers and of Ag atoms to the Bi layer formed on the Ag surface (see figure 11 c). Surprisingly but not unexpected, the atomic migration maintains the cubic phase rearrangement in both, the Ag surface and the new Bi layer deposited on the Ag surface. In comparison with the structure of the interface without doping atom, the interface doped in the third layer does not display significative differences in the region near to the contact between both surfaces. Being the doped layer surface the most stable of the Ag doped interfaces, the optimized structure of the interface helps us to understand some interesting aspects of how the interface can facilitate the Ag-Bi BN formation. The interatomic distances between the Ag atoms bonded to the Bi atom are very similar to that found in the Ag bulk, then the interface not only helps to stabilize the system by the strong interaction among the Bi and Ag atoms in the interface (structure which does not display significative difference with the undoped interface) but also in some way stabilizes the Bi atoms inside the Ag bulk structure. The second fact is related to the relative stability of the third doped layer interface in comparison with the interface doped in the more superficial layers. No matter what can occur due to the interface formation (e.g. the interface doped in the second layer produced a strong distortion in the interface even migration of Ag atoms to the Bi substrate) a very crystalline Ag-Bi nanoalloy in cubic phase will be the more stable situation from a thermodynamic point of view.

To validate if the energetic behavior obtained in the interface does not depend of the surface vectors used to built the interface, segregation energies were calculated in a clean surface of Ag with the same surface vectors of the interface. As shown in figure 12, the segregation energies calculated in both surfaces are similar assuring that changes in the segregation energies obtained when the Ag surface was doped with a Bi atom at the interface occurred due to the interface formation and not for the changes on the surface vectors. Then, our results are in good concordance with experimental findings; if an interface Ag-Bi is reached, it is more stable the formation of nanoalloys of Ag in cubic phase doped with Bi atoms.

## STRUCTURAL EFFECTS DUE TO THE NANOALLOY FORMATION

Ag-Bi BNs formation is undoubtedly a dynamic process. As the doping atoms replace the atoms in the crystal network, the cell reconstruction must occur until reach the more stable configuration under a specific doping concentration. Experimental studies focus to determine the concentration of the Bi on BNs in a cubic phase of Ag obtained by a fs laser beam, showed that stable nanoalloys were found with a concentration of 6 ± 1 atom % and the doping produces an increment of 4.2 %. in the interplanar distances in direction of the (111) planes [35]. On the other hand, the Ag substitutes the Bi atoms producing stable nanoalloys for Ag molar fractions smaller than 0.2 to 0.3 inducing a contraction of

the Bi matrix [31]. Then, it is interesting to see if our methodology is able to reproduce the structural changes suffered in the bulk cells of these materials when they are doped. Since a unit cell of Ag in a cubic phase has four atoms, for representing the Bi percent in the Ag cubic phase it is necessary to increase the unit cell volume. In a 2x2x2 supercell of the Ag unit cell, two Bi atoms are enough to reach the concentration observed experimentally. With the objective to maintain the cubic phase, the substitutions were carried out in the center and in the vertices of the supercell which leads exactly to two Bi atoms. In turn, the unit cell of the hexagonal Bi has six atoms so that the substitution of one Bi atoms by one Ag is enough to reach the observed experimental concentration. Figure 13 and Table 2 display the structures and the cell parameters of the optimized doped cells. Doping the hexagonal unit cell of Bi with one Ag atom produce a decreasing in the cell parameters, being more significative in the "c" direction. Taking as reference the optimized parameters without doping, the reduction in the "a" and "c" parameters are 1 and 11 %, approximately. The strong change suffers in the c direction is due to an increasing in the interaction distances between the Bi bilayers which are exactly parallel to the (001) direction. Since all the Bi atoms have the same coordination inside the hexagonal bulk, at this concentration (approximately 17 %) the substitution of any Bi atom in the bulk must lead to the same changes in the cell parameters. Unlike the observed in the Bi bulk and in good accordance with the experimental findings, the Ag bulk doped with Bi atoms displays a slight increased in the cell parameters. Larger cell parameters induce, as expected, larger distances between the planes present in the nanoalloys as has been determined by means of HR-TEM images in Ref. 35. From the HR-TEM studies was determined that the separation distance between the (111) planes of the Ag-Bi nanoalloys was 2.46 Å which compared with the value obtained of 2.43 Å in our Ag doped bulk, is only 1 % higher. Then, the results obtained in this work are, also from a structural point of view, in good concordance with the experimental observation in relation to the changes occurs when bulks of Bi or Ag are doped with Ag and Bi, respectively.

Figure 6 displays the segregation energy of the Bi or Ag atom in the clean surfaces and the interface. Segregation energies indicate that in clean surfaces, the doping atoms prefer placed near the surface, top and second layer for the Ag and Bi surfaces, respectively. Interestingly, the interface formation does not change the qualitative aspect of the segregation energy in the Bi surface but it does in the Ag surface, that is, the Bi atoms prefer to go to the bulk of the Ag cubic phase when an interface is formed. These results agree reasonably with two experimental facts. Because of the doping atoms prefer the more external layers of Ag or Bi surfaces, the Ag-Bi BNs are very difficult to synthesize. The second fact is that under laser fs conditions where an interface Ag-Bi is formed, only the presence of BNs of Ag in cubic phase doped with Bi has been detected. With the aim to understand why the interface produces this change on the Ag surface, we are going to analyze in detail the structure surrounding the doping atom in both the clean surfaces and the interface.

## CONCLUSIONS

A DFT approach in the context of GGA approximation has been used to determine the structural and energetic changes produced in the formation of Ag-Bi BNs. This approximation showed to be good enough to simulate the structural changes suffered by the bulks of Ag and Bi when they are doped with specific concentrations of Bi and Ag, respectively. In the hexagonal Bi bulk and at low concentrations (less than a concentration of 0.2 molar fraction), Ag atoms tend to reduce the interaction between the Bi bilayers which considerably decreases "c" vector maintained practically unaltered the others vectors of the cell. The differences in electronic density distribution and the *d* orbital of the Ag atoms seem to play a crucial role in why the Ag atoms look to interact at shorter distances with the Bi atoms. On the other hand, Bi atoms in the Ag bulk structure produce an expansion but they do not have problems to adopt the cubic phase structure even at the interface formation due to the increasing disordering.

Segregation energies studies in clean surfaces and in an interface formed with these surfaces are in good agreement with the experimental findings, when an Ag-Bi interface is formed the more favorable situation is the formation of a BN of Ag in cubic phase doped with Bi. The interface changes the stability of the system helping the Bi atoms to go inside the extremely compact Ag bulk, however, the strong interaction between the Ag and Bi surfaces, when the interface is formed, produces strong changes in the less dense Bi structure making less favorable that Ag atoms go inside the Bi bulk structure, even in some cases, the bulk structure of the Bi surface is lost completely. In clean surfaces, segregation energies showed that doping atoms prefer to be in the surface which is in good agreement with the fact that the immiscibility of these materials is very low. However, in a contracted Bi cell the Ag atoms could stabilize the system making feasible the formation of a Bi BN doped with Ag.

REFERENCES

1.- Julius Jellinek. Nanoalloys: tuning properties and characteristics through size and composition. Faraday Discuss., 2008, 138, 11–35.

2.- Riccardo Ferrando, Julius Jellinek, and Roy L. Johnston. Nanoalloys: From Theory to Applications of Alloy Clusters and Nanoparticles. Chemical Reviews, 2008, 108, 3, 845-910.

3.- Nanoalloys: From Fundamentals to Emergent Applications, ed. F. Calvo, Elsevier, 2013.

4.- Florent Calvo. Thermodynamics of nanoalloys. Phys. Chem. Chem. Phys., 2015, 17, 27922-27939.

5.- Hai-Long Jiang and Qiang Xu. Recent progress in synergistic catalysis over heterometallic nanoparticles. *J. Mater. Chem.*, 2011, 21, 13705.

6.- Danielle A. Hansgen, Dionisios G. Vlachos and Jingguang G. Chen. Using first principles to predict bimetallic catalysts for the ammonia decomposition reaction. *Nature Chemist*ry volume 2, pages 484–489 (2010).

7.- F. Studt, F. Abild-Pedersen, T. Bligaard, R. Z. Sørensen, C. H. Christensen, J. K. Nørskov, *Science* 2008, 320, 1320 –1322.

8.- Hu, X.; Zhao, Y.; Hu, Z.; Saran, A.; Hou, S.; Wen, T.; Liu, W.; Ji, Y.; Jiang, X.; Wu, X. Gold Nanorods core/AgPt Alloy Nanodots Shell: A Novel Potent Antibacterial Nanostructure. *Nano Res*. 2013, 6, 822−835.

9.- Paszkiewicz, M.; Gołąbiewska, A.; Rajski, Ł.; Kowal, E.; Sajdak, A.; Zaleska-Medynska, A. Synthesis and Characterization of Monometallic (Ag, Cu) and Bimetallic Ag-Cu Particles for Antibacterial and Antifungal Applications. *J. Nanomater*. 2016, 2016, No. 2187940.

10.- Padmos, J. D.; Langman, M.; Macdonald, K.; Comeau, P.; Yang, Z.; Filiaggi, M.; Zhang, P. Correlating the Atomic Structure of Bimetallic Silver Gold Nanoparticles to Their Antibacterial and Cytotoxic Activities. *J. Phys. Chem. C* 2015, 119, 7472−7482.

11.- Shiyao Shan, Jin Luo, Lefu Yang† and Chuan-Jian Zhong. Nanoalloy catalysts: structural and catalytic properties. Catal. Sci. Technol., 2014, 4, 3570–3588.

12.- Shiyao Shan, Jin Luo, Jinfang Wu, Ning Kang, Wei Zhao, Hannah Cronk, Yinguang Zhao, Pharrah Joseph, Valeri Petkov and Chuan-Jian Zhong. RSC Adv., 2014, 4, 42654–42669.

13.- Kyle D. Gilroy, Aleksey Ruditskiy, Hsin-Chieh Peng, Dong Qin, and Younan Xia. Bimetallic Nanocrystals: Syntheses, Properties, and Applications. Chem. Rev. 2016, 116, 10414−10472.

14.- Jun Meng, Beien Zhu, and Yi Gao. Surface Composition Evolution of Bimetallic Alloys under Reaction Conditions. J. Phys. Chem. C 2019, 123, 28241−28247.

15.- Jocelyn T. L. Gamler, Alberto Leonardi, Hannah M. Ashberry, Nicholas N. Daanen,

Yaroslav Losovyj, Raymond R. Unocic, Michael Engel, and Sara E. Skrabalak. Achieving Highly Durable Random Alloy Nanocatalysts through Intermetallic Cores. ACS Nano 2019, 13, 4008−4017.

16.- Emil Roduner. Size matters: why nanomaterials are different. Chem. Soc. Rev., 2006, 35, 583–592.

17.- M. Bruchez , M. Moronne , P. Gin , S. Weiss , A. P. Alivisatos , Science 1998 , 281 , 2013.

18.- M. A. El-Sayed , Acc. Chem. Res. 2004 , 37 , 326.

19.- J. F. Parker , C. A. Fields-Zinna , R. W. Murray , Acc. Chem. Res. 2010 , 43 , 1289.

20.- S. E. Habas , H. Lee , V. Radmilovic , G. A. Somorjai , P. Yang , Nature Mater. 2007 , 6 , 692.

21.- D. Xu , Z. P. Liu , H. Z. Yang , Q. S. Liu , J. Zhang , J. Y. Fang , S. Z. Zou , K. Sun , Angew. Chem. Int. Ed. 2009 , 48 , 4217.

22.- Andrews, M. P.; O'Brien, S. C. Gas-phase "molecular alloys" of bulk immiscible elements: iron-silver (FexAgy). J. Phys. Chem. 1992, 96, 8233−8241.

23.- Christensen, A.; Stoltze, P.; Nørskov, J. K. Size dependence of phase separation in small bimetallic clusters. J. Phys.: Condens. Matter 1995, 7, 1047−1057.

24.- Xia, F.; Xu, X.; Li, X.; Zhang, L.; Zhang, L.; Qiu, H.; Wang, W.; Liu, Y.; Gao, J. Preparation of bismuth nanoparticles in aqueous solution and its catalytic performance for the reduction of 4- nitrophenol. Ind. Eng. Chem. Res. 2014, 53, 10576−10582.

25.- Dong, F.; Li, Q.; Zhou, Y.; Sun, Y.; Zhang, H.; Wu, Z. In situ decoration of plasmonic Ag nanocrystals on the surface of (BiO)2CO3 hierarchical microspheres for enhanced visible light photocatalysis. Dalton Trans. 2014, 43, 9468−9480.

26.- Wenjing, L. Site synthesis of bismuth nanoparticles for electrochemical determination of lead. Micro Nano Lett. 2012, 7, 1260−1263.

27.- Rastogi, P. K.; Ganesan, V.; Krishnamoorthi, S. A promising electrochemical sensing platform based on a silver nanoparticle decorated copolymer for sensitive nitrite determination. J. Mater. Chem. A 2014, 2, 933−943.

28.- De, M.; Ghosh, P. S.; Rotello, V. M. Applications of nanoparticles in biology. Adv. Mater. 2008, 20, 4225−4241.

29.- Hernandez-Delgadillo, R.; Velasco-Arias, D.; Diaz, D.; Arevalo- Niño, K.; Garza-Enriquez, M.; De la Garza-Ramos, M. A.; Cabral- Romero, C. Zerovalent bismuth nanoparticles inhibit Streptococcus mutans growth and formation of biofilm. Int. J. Nanomed. 2012, 7, 2109−2113.

30.- Karakaya, I.; Thompson, W. T. The Ag-Bi (silver-bismuth) system. J. Phase Equilib. 1993, 14, 525−529.

31.- Víctor-Fabián Ruiz-Ruiz, Inti Zumeta-Dubé, David Díaz, M. Josefina Arellano-Jiménez, and Miguel José-Yacamán. J. Phys. Chem. C 2017, 121, 940−949.

32.- Longo, E.; Volanti, D. P.; Longo, V. M.; Gracia, L.; Nogueira, I. C.; Almdeira, M. A. P.; Pinheiro, A. N.; Ferrer, M. M.; Cavalcante, L. S.; Andrés, J. Toward an Understanding of the Growth of Ag Filaments on α-Ag2WO4 and Their Photoluminescent Properties: A Combined Experimental and Theoretical Study. J. Phys. Chem. C 2014, 118, 1229−1239.

33.- de Oliveira, R. C.; Zanetti, S. M.; Assis, M.; Penha, M.; Mondego, M.; Cilense, M.; Longo, E.; Cavalcante, L. S. Effect of Metallic Ag Growth on the Electrical Resistance of 3D Flower-like Ag4V2O7 Crystals. J. Am. Ceram. Soc. 2017, 100, 2358−2362.

34.- Assis, M.; Cordoncillo, E.; Torres-Mendieta, R.; Beltrán-Mir, H.; Minguez-Vega, G.; Gouveia, A. F.; Leite, E.; Andrés, J.; Longo, E. Laser-Induced Formation of Bismuth Nanoparticles. Phys. Chem. Chem. Phys. 2018, 13693−13696.

35.- Thales R. Machado, Nadia G. Macedo, Marcelo Assis, Carlos Doñate-Buendia, Gladys Mínguez-Vega, Mayara M. Teixeira, Camila C. Foggi, Carlos E. Vergani, Héctor Beltrán-Mir, Juan Andrés, Eloisa Cordoncillo, and Elson Longo. ACS Omega 2018, 3, 9880−9887.

36.- Lida Farsi and N. Aaron Deskins. First principles analysis of surface dependent segregation in bimetallic alloys. Phys.Chem.Chem.Phys., 2019, 21, 23626.

37.- Giovanni Di Liberto, Sergio Tosoni and Gianfranco Pacchioni. Phys.Chem.Chem.Phys., 2019, 21, 21497.

38.- Bing-Joe Hwang, Loka Subramanyam Sarma, Jiun-Ming Chen, Ching-Hsiang Chen, Shou-Chu Shih, Guo-Rung Wang, Din-Goa Liu, Jyh-Fu Lee, and Mau-Tsu Tang. Structural Models and Atomic Distribution of Bimetallic Nanoparticles as Investigated by X-ray Absorption Spectroscopy. J. AM. CHEM. SOC. 9 VOL. 127, NO. 31, 2005 11141 .

39.- Miaofang Chi, Chao Wang, Yinkai Lei, Guofeng Wang, Dongguo Li, Karren L. More, Andrew Lupini, Lawrence F. Allard, Nenad M. Markovic & Vojislav R. Stamenkovic. Surface faceting and elemental diffusion behavior at atomic scale for alloy nanoparticles during in situ annealing. Nature Communications volume 6, Article number: 8925 (2015).

40.- Shuxin Wang, Qi Li, Xi Kang, and Manzhou Zhu. Customizing the Structure, Composition, and Properties of Alloy Nanoclusters by Metal Exchange. Acc. Chem. Res. 2018, 51, 2784−2792.

41.- Qiaofeng Yao, Yan Feng, Victor Fung, Yong Yu, De-en Jiang, Jun Yang & Jianping Xie. Precise control of alloying sites of bimetallic nanoclusters via surface motif exchange reaction. Nat. Commun. 2017, 8, 1555.

42.- G. Kresse, J. Hafner, Phys. Rev. B: Condens. Matter 47 (1993) 558–561.

43.- G. Kresse and J. Furthmüller, “Efficient iterative schemes for ab initio total energy calculations using a plane-wave basis set,” Phys. Rev. B 54, 11169–11186 (1996).

44.- J. P. Perdew, K. Burke, and M. Ernzerhof, “Generalized gradient approximation made simple,” Phys. Rev. Lett. 77, 3865–3868 (1996).

45.- P. Blöchl, Phys. Rev. B: Condens. Matter 50 (1994) 17953–17979.

46.- G. Kresse, D. Joubert, Phys. Rev. B: Condens. Matter 59 (1999) 1758–1774.

47.- In-Kook Suh, H. Ohta, Y.Waseda. High-temperature thermal expansion of six metallic elements measured by dilatation method and X-ray diffraction. JOURNAL OF MATERIALS SCIENCE 23 (1988) 757-760.

48.- BY D. SCHIFERL AND C. S. BARRETT. The Crystal Structure of Arsenic at 4·2, 78 and 299 °K. J. Appl. Cryst. (1969). 2, 30.

49.- Matej Huš, Anders Hellman. Ethylene Epoxidation on Ag(100), Ag(110), and Ag(111): A Joint Ab Initio and Kinetic Monte Carlo Study and Comparison with Experiments. ACS Catal. 2019, 9, 2, 1183-1196.

50.- Liyan Zhu, Tingting Zhang, and Jinlan Wang. Electronic Structure of Bi Nanoribbon: Greatly Influenced by Edge Chirality and Edge Reconstruction. J. Phys. Chem. C 2010, 114, 19289–19293.

51.- Y. Yu, W. Xiao, J. Wang and L. Wang, Materials, 2016, 9, 5.

52.- Yanlin Yu, Wei Xiao, Jianwei Wang and Ligen Wang. Phys.Chem.Chem.Phys., 2016, 18, 26616.

53.- Ph. Hofmann. The surfaces of bismuth: Structural and electronic properties. Progress in Surface Science 81 (2006) 191–245.

54.- Liyan Zhu, Tingting Zhang, and Jinlan Wang. Electronic Structure of Bi Nanoribbon: Greatly Influenced by Edge Chirality and Edge Reconstruction. J. Phys. Chem. C 2010, 114, 19289–19293.

55.- S. Varga, S. Varga, H. Nakamatsu, T. Mukoyama, J. Anton, D. Geschke, A. Heitmann, E. Engel, T. Bastuğ. Four-component relativistic density functional calculations of heavy diatomic molecules. J. Chem. Phys., Vol. 112, No. 8, 22 February 2000.

56.- Lide, D. R. CRC Handbook of Chemistry and Physics; CRC Press: Boca Raton, FL, 2005.

57.- Karakaya, I.; Thompson, W. T. The Ag-Bi (silver-bismuth) system. J. Phase Equilib. 1993, 14, 525−529.

Table 1. Experimental and calculated bulk parameters for the hexagonal and cubic phases of Bi and Ag, respectively. Distances in Å.

| | Cubic Ag | Hexagonal Bi | |
|---|---|---|---|
| | a=b=c | a=b | c |
| Experimental | 4.086 | 4.546 | 11.862 |
| Calculated | 4.147 | 4.580 | 12.135 |
| Error (%) | 1.5 | < 1 | 2.3 |

Table 2. Optimized bulk parameters for the doped hexagonal and cubic phases of the Bi and Ag, respectively. Distances in Å.

| | Cubic Ag | Hexagonal Bi | |
|---|---|---|---|
| | a=b=c | a=b | c |
| Doped | 8.410 | 4.520 | 10.810 |
| Calc. | 8.294 | 4.580 | 12.135 |

Figure 1. Top (right) and lateral (left) views of the (100) surfaces. A) a 2x3 slab of the Ag cubic phase and B) 2x1 slab of the Bi hexagonal phase

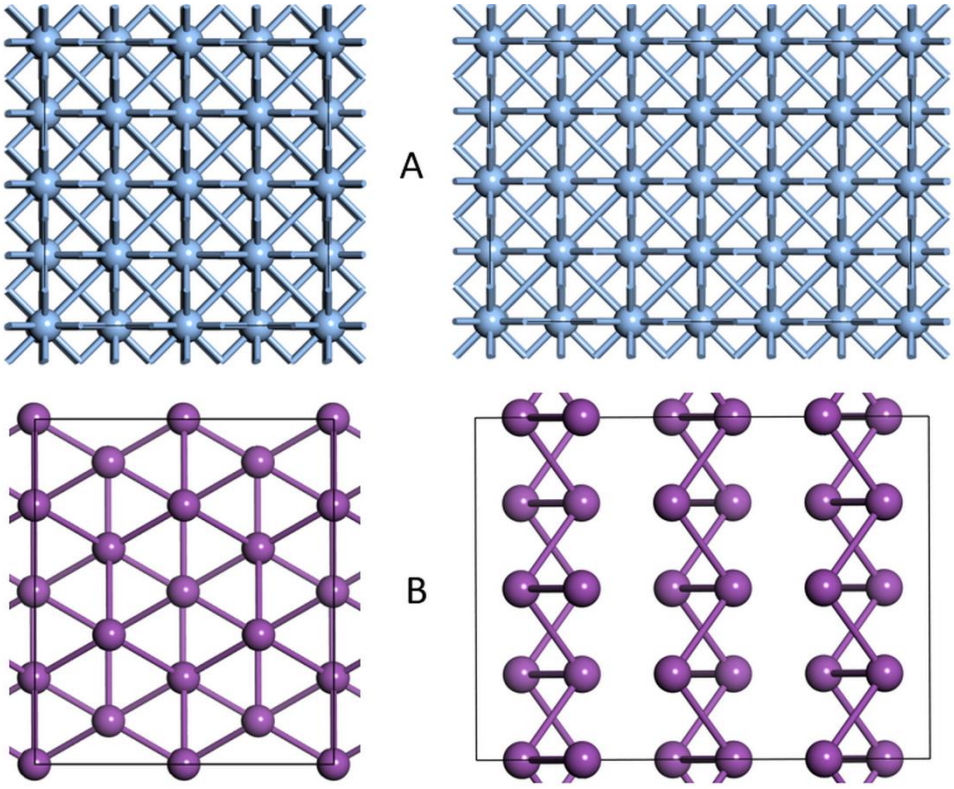

Figure 2. Values of structural parameters for the Bi (100) surface. In normal text the non-optimized surface, in italic text the slab with 9 layers and in underline text the slab with 16 layers. For a better overview, a 2x1.5 cell with nine layers was depicted. Distances in Å and angles in degrees

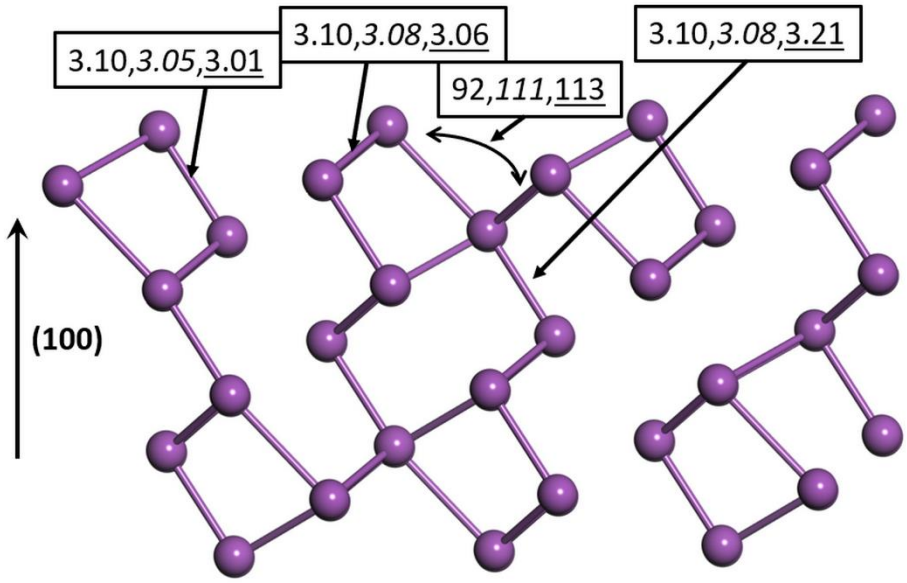

Figure 3. Non optimized (left) and optimized (right) structure of the interface formed with the five layers Ag (100) surface and the nine layers Bi (100) surface, respectively. Distances in Å

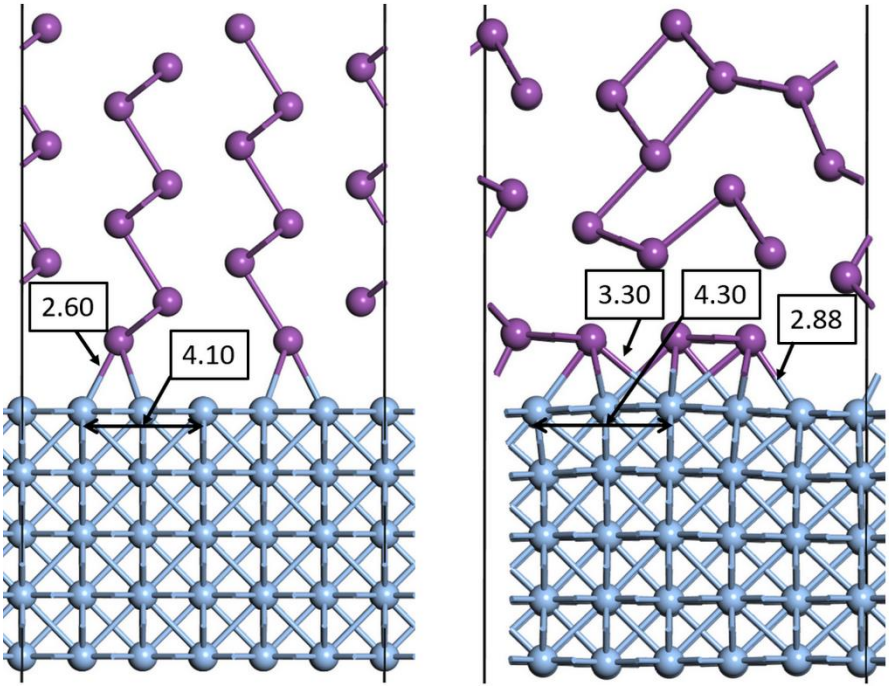

Figure 4. Number of interaction with distances less than 3.7 Å for the bulk (black lines), clean surface (red lines) and the Bi slab at the interface (blue lines).

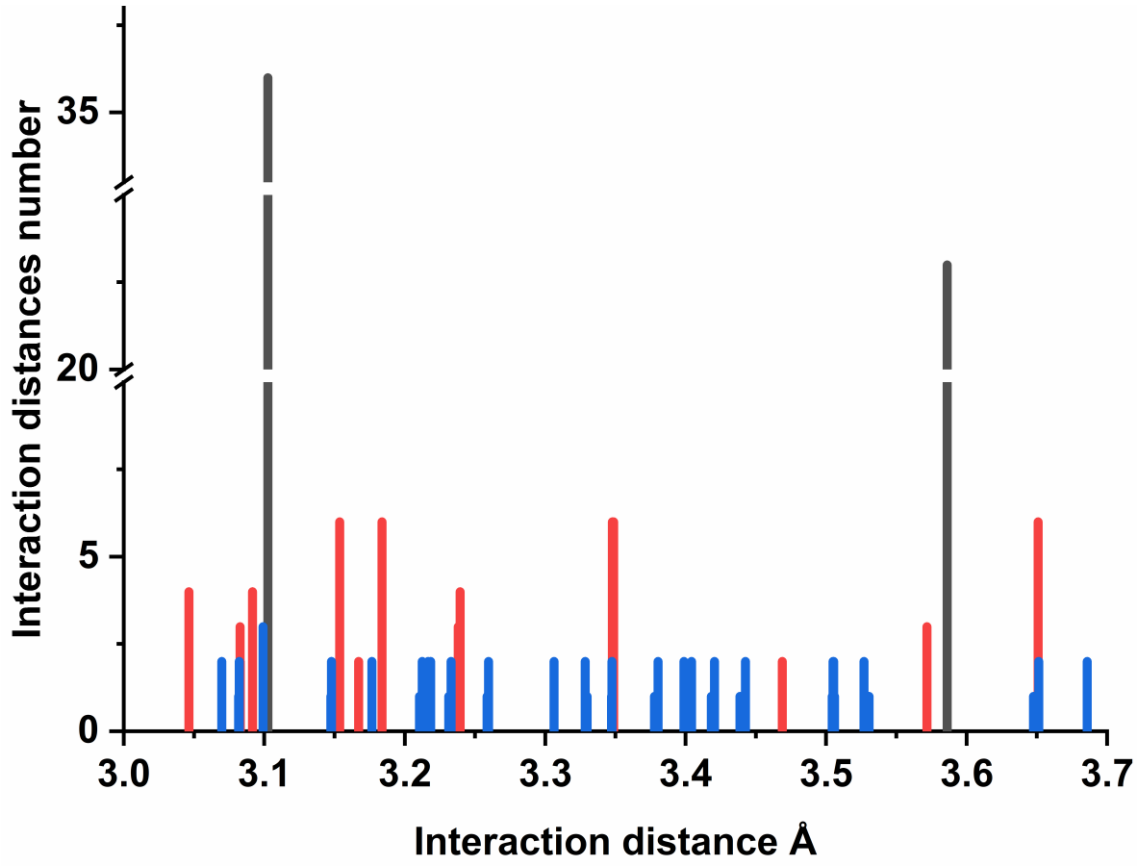


Figure 5. DOS of the Ag and Bi bulks, (100) clean surfaces and interface

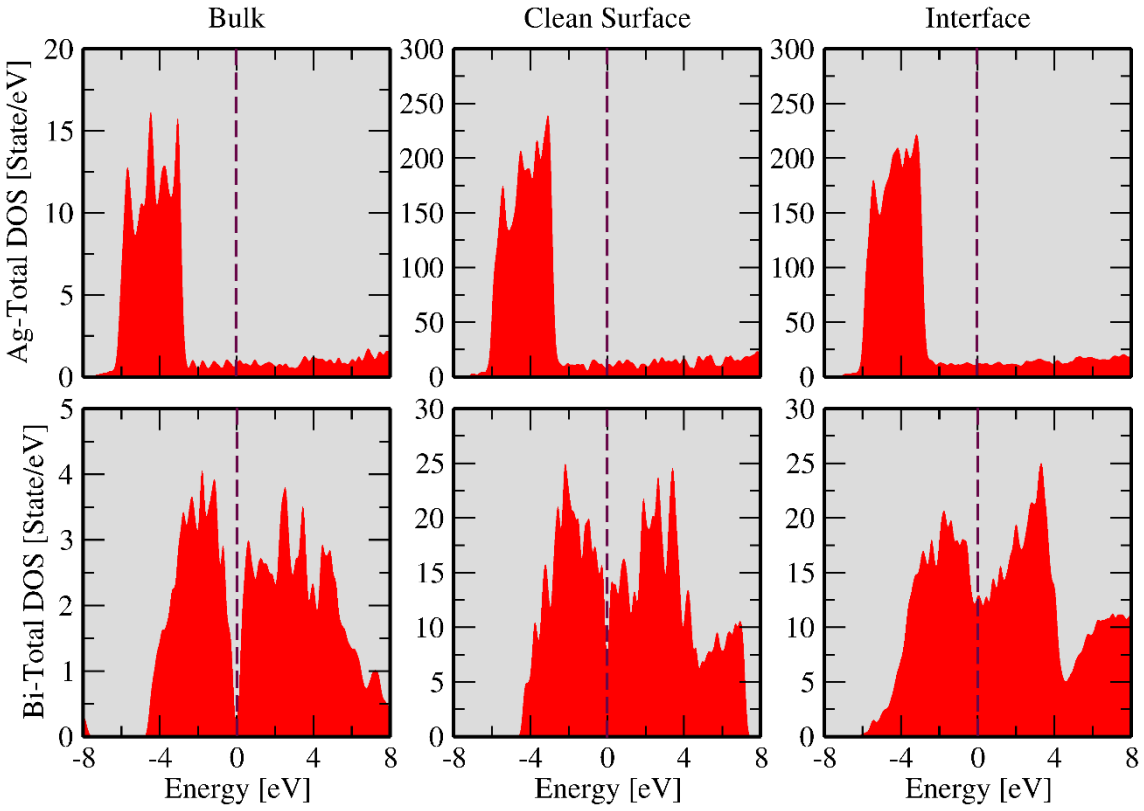
Bulk
Clean Surface
Interface
Ag-Total DOS [State/eV]
Bi-Total DOS [State/eV]
Energy [eV]
Energy [eV]
Energy [eV]

Figure 6. Segregation energy of Ag in a clean surface of Bi (black line) and in the Bi surface at the interface (red line)

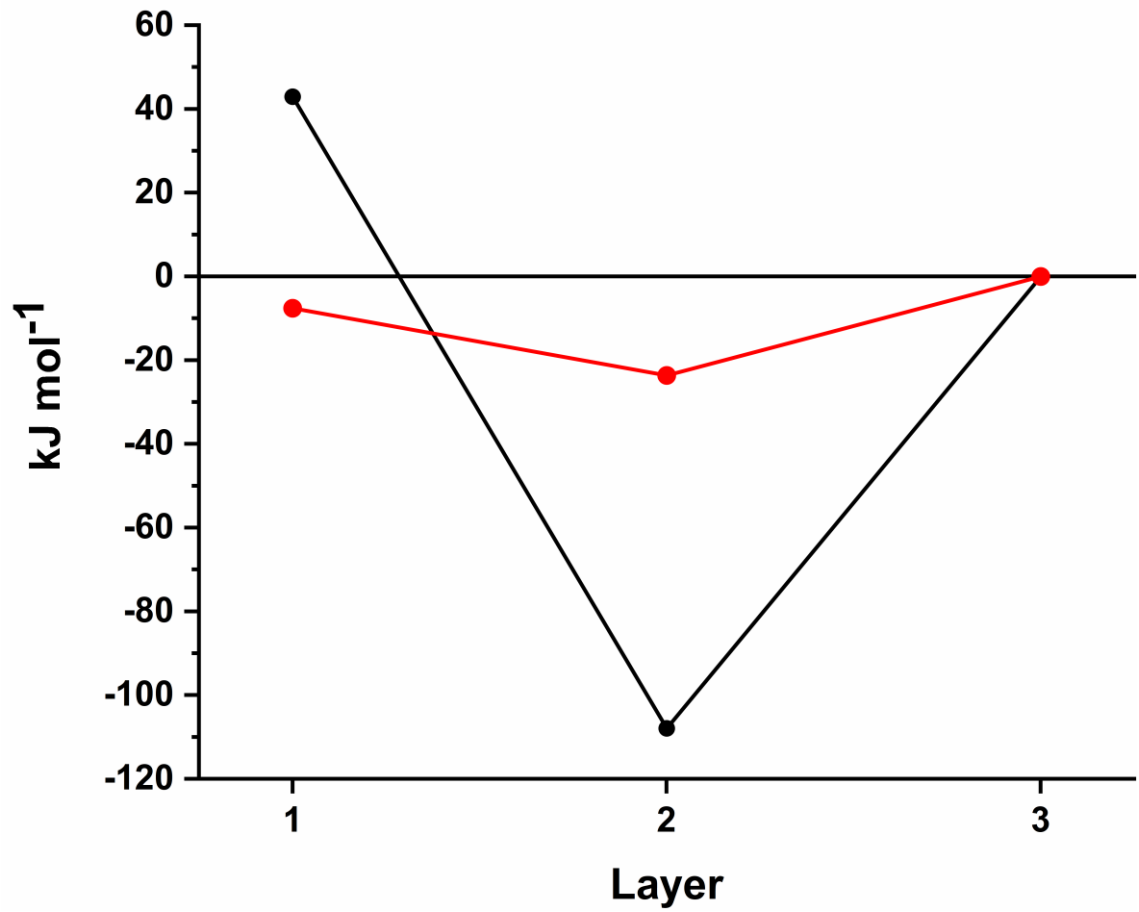

Figure 7. Lateral views of the optimized structures for the Bi surface doped at the first (b), second (c) and third (d) layer with an Ag atom. For comparison purposes, the optimized structure of the undoped surface has been depicted (a)

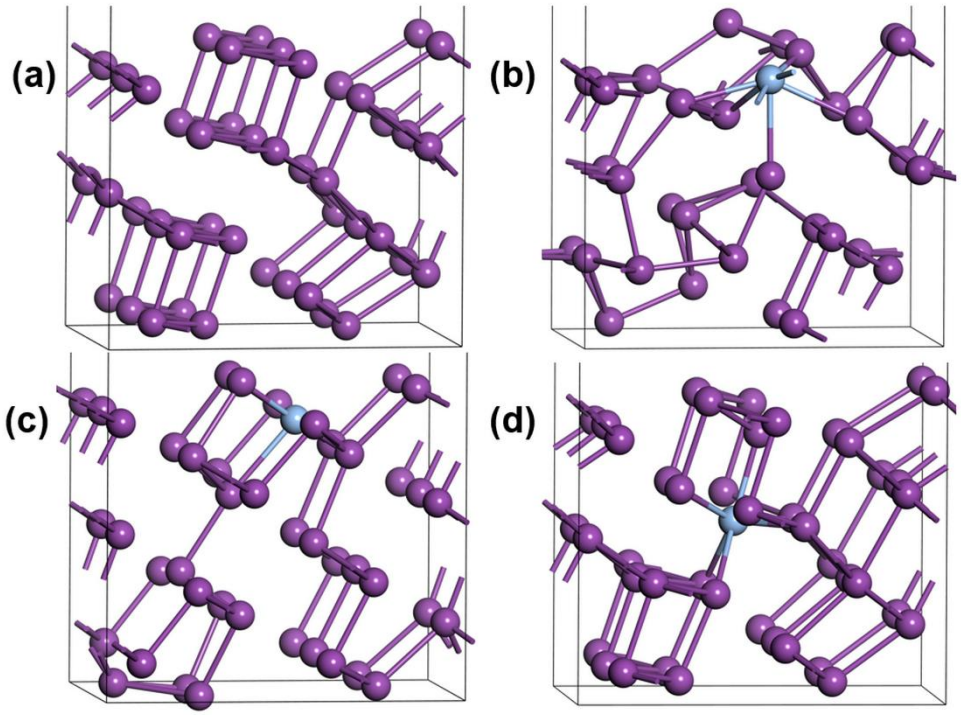

Figure 8. Lateral views of the optimized structures for the interface doped with an Ag atom in the first (b), second (c) or third (d) Bi layer. For comparison purposes, the clean interface was depicted (a). For a better overview, the interface doped in the second and third layers were rotated 180 °and only the two upper layers of the Ag surface were displayed.

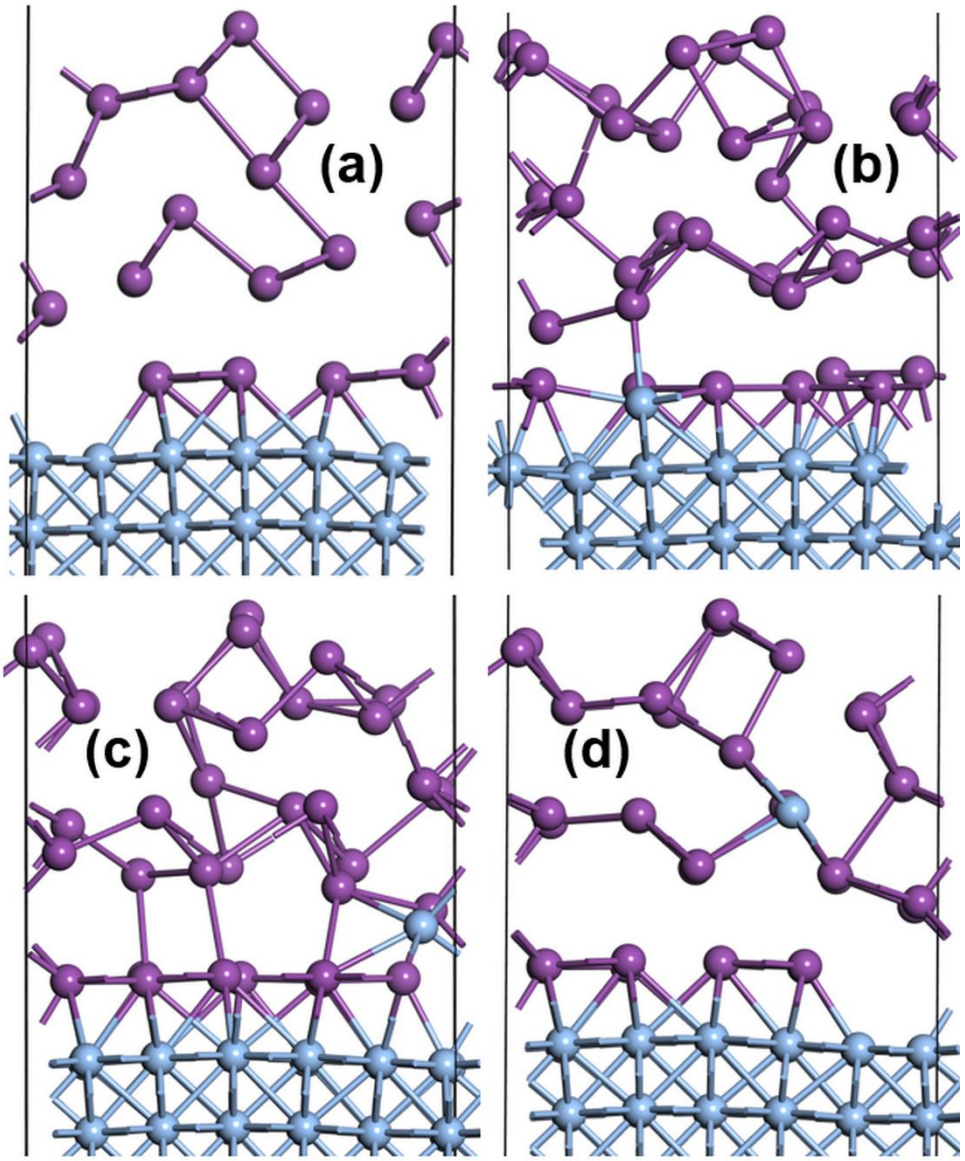

Figure 9. Segregation energy of Bi in a clean surface of Ag (black line) and in the Ag surface at the interface (red line)

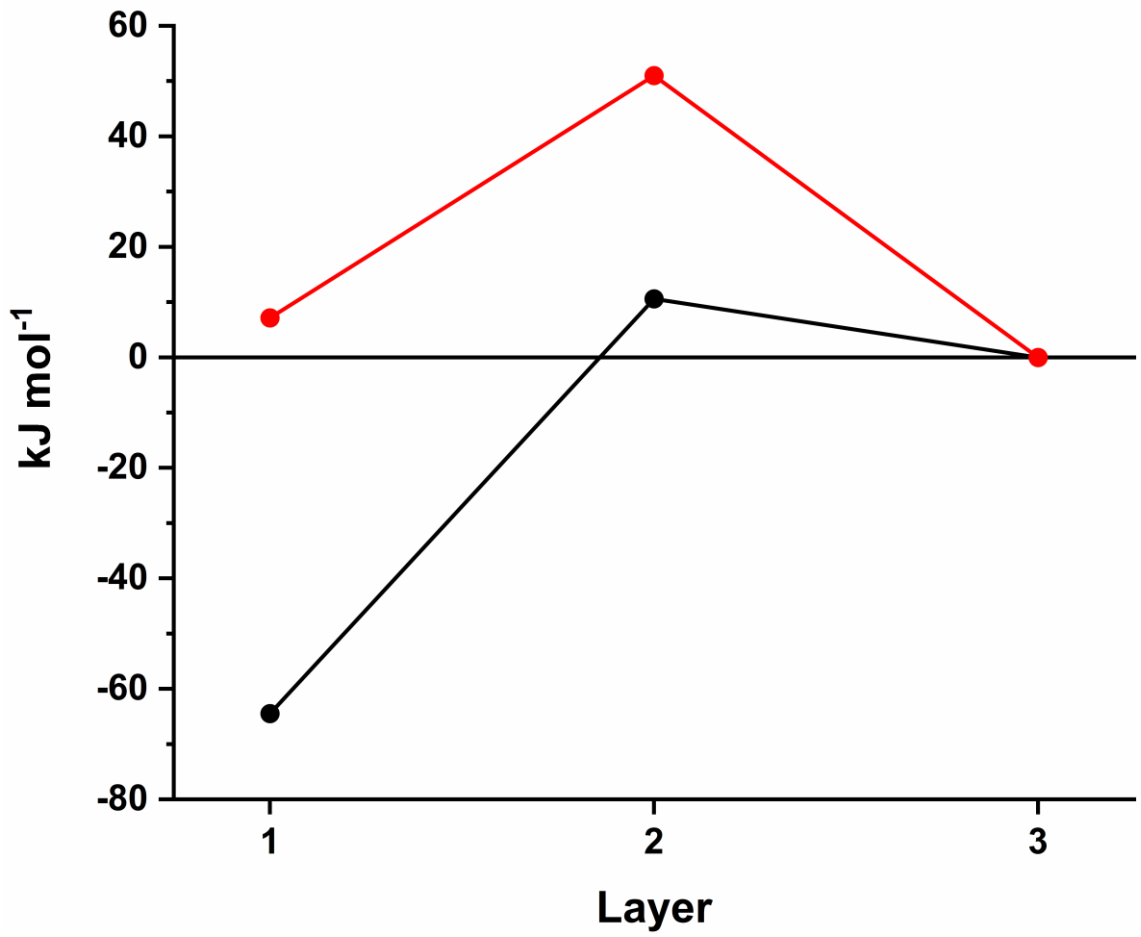

Figure 10. Lateral view of the optimized structures for the substitution process of one Ag atom by one Bi atom in the first (a), second (b) and third (c) layer of a clean Ag (100) surface. For a better overview, the cell was cut such as the Bi atom was exposed and only the nearest atoms were depicted.

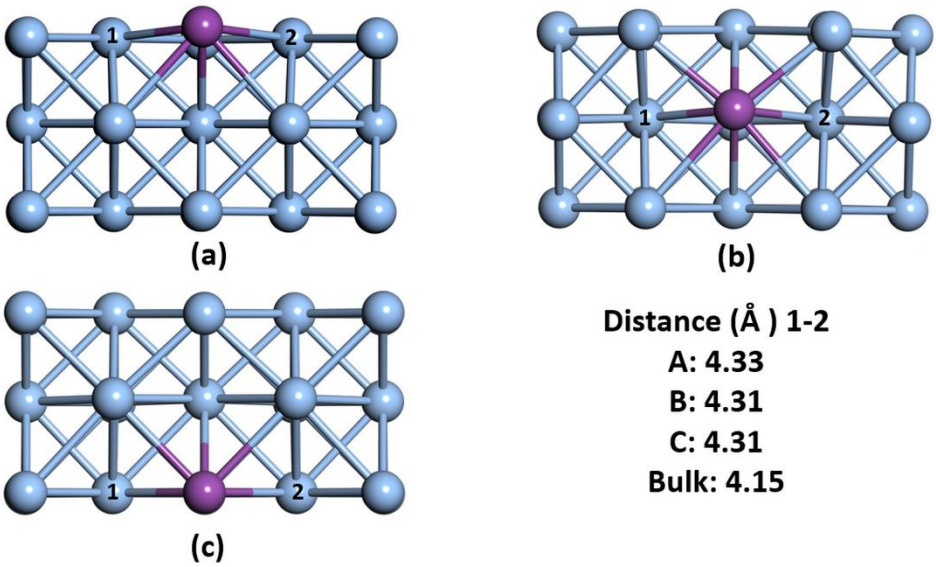

Figure 11. Lateral views of the optimized structures for the interface doped with a Bi atom in the first (b), second (c) or third (d) Bi layer. For comparison purposes, the clean interface was displayed (a). For a better overview, the interface doped in the third layer was rotated 180°.

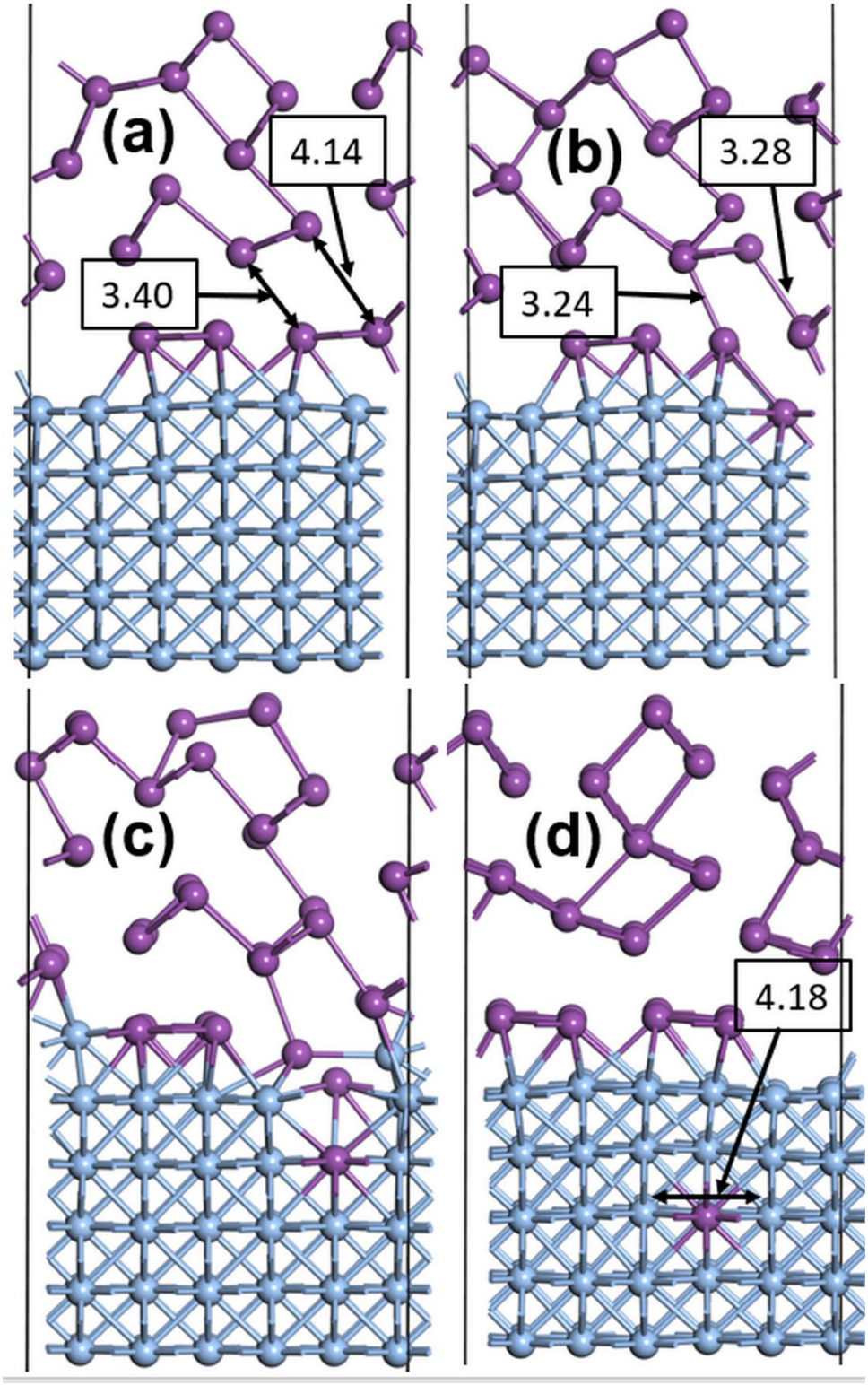

Figure 12. Segregation energies in Ag (100) clean surfaces with surface vectors of the Ag cubic phase (red line) and the interface (black line)

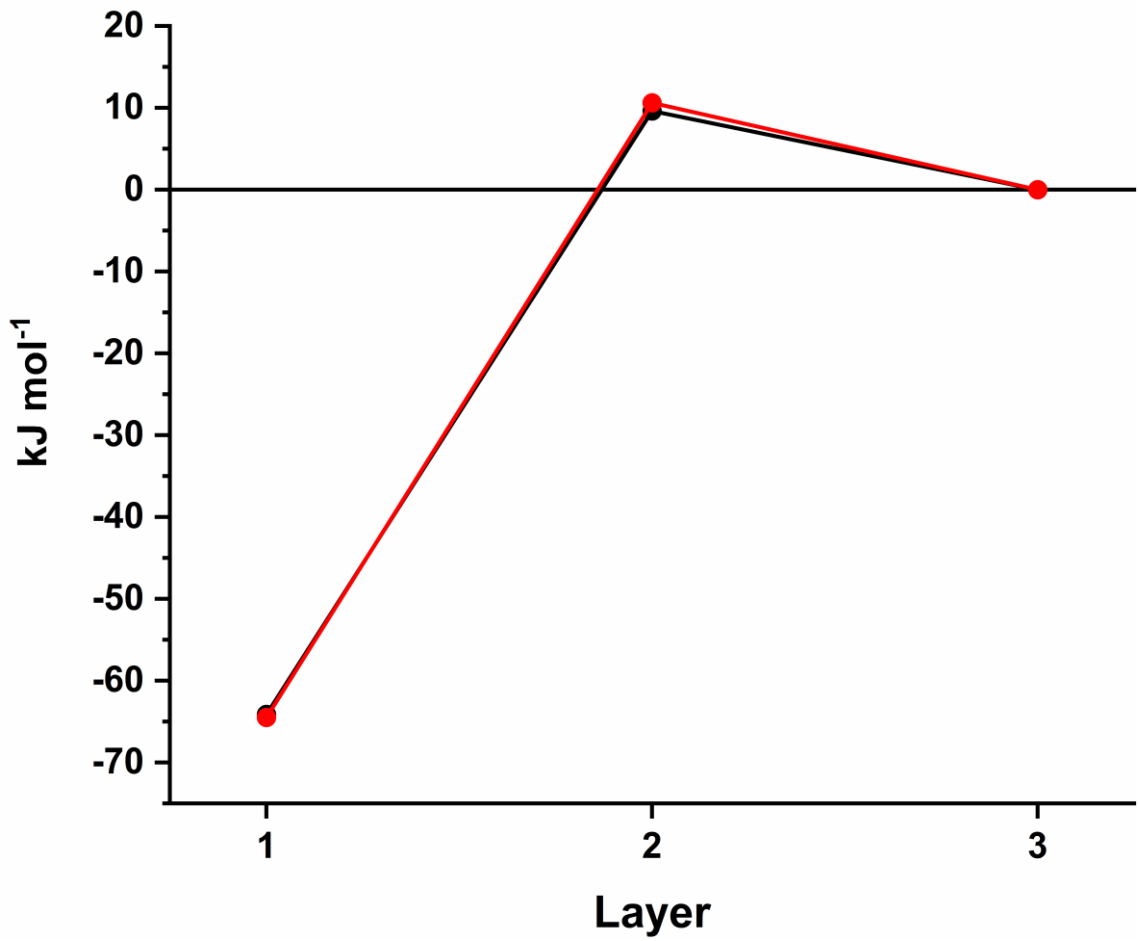

Figure 13. Optimized structures for the doped Ag cubic (left) and Bi hexagonal (right) phases